Applied Catalysis A, General 711 (2026) 120744

Contents lists available at ScienceDirect

Applied Catalysis A, General

journal homepage: www.elsevier.com/locate/apcata

Direct oxidative carbonylation of waste methane to acetic acid over Rh/zeolite catalysts

Jialin Yu [a], Olukayode Gideon Oloyede [a], Mark B.F. Berko [b], Kunlun Ding [b], Richard J. Lewis [c], Stuart H. Taylor [c], Graham J. Hutchings [c,*], Kang Li [a], David Chadwick [a,*]

[a] Department of Chemical Engineering, Imperial College London, South Kensington, London SW7 2AZ, UK
[b] Department of Chemical Engineering, Louisiana State University, Baton Rouge, LA 70803, USA
[c] Max Planck, Cardiff Centre on the Fundamentals of Heterogeneous Catalysis FUNCAT, Cardiff Catalysis Institute, School of Chemistry, Cardiff University, Cardiff CF24 4HQ, UK

ARTICLE INFO

Keywords:
Oxidation
Methane
Acetic acid
Rh
ZSM-5

ABSTRACT

Direct oxidation of methane to oxygenates remains challenging in heterogeneous catalysis. In this work, direct oxidative carbonylation of low-concentration methane to acetic acid has been investigated over Rh/zeolite catalysts. Formation of acetic acid over Rh/ZSM-5 is shown to be far superior compared to a range of other Rh/zeolite catalysts, including Rh/Z-beta, Rh/Z-Y, Rh/Mor, Rh/Fer, and Rh/SSZ-13. The importance of the 3D channel structure of ZSM-5 is emphasised by a comparison with unidirectional Rh/ZSM-23 which showed much lower production of acetic acid. Acetic acid production is found to be maximum at a SiO_2/Al_2O_3 ratio corresponding to ZSM5–50. Isolated Rh is identified as the active site for liquid oxygenate production with 0.09 wt% Rh/ZSM5 giving the highest acetic acid production. Higher Rh loading leads to a drop in production due to the gradual formation of Rh nanoparticles. Acetic acid production is shown to be strongly pressure dependent consistent with 2nd or higher order apparent kinetics compared to apparent 1st order for C1 products. Competing direct CO oxidation to CO_2 was responsible for above 85 % of the total CO_2 production. These findings highlight the critical role of zeolite topology in enhancing selective methane valorisation over Rh catalysts, and provide insights into developing practical catalytic processes for low-carbon chemical manufacturing.

1. Introduction

Methane is a powerful greenhouse gas and the second largest contributor to global warming [1]. Reducing methane emissions is, therefore, an important strategy in the mitigation of climate change and thus the development of feasible technologies to remove and utilise waste methane, especially low-concentration methane (technically defined as lower than 30 %) arising for example from depleted natural gas wells, lean streams from biogas upgrading etc [2,3], is essential. The indirect route of methane conversion to platform chemicals via synthesis gas is highly engineered and is a key process in the chemical industry. However, the processes involved are generally equilibrium-limited and endothermic, consuming large amounts of energy. In contrast, the direct conversion of methane to produce C1 and C2 oxygenated products is generally exothermic and irreversible, and as such offers a more sustainable approach to the utilisation of waste methane. However, the direct route continues to be a challenge to catalysis, since methane is essentially an inert gas and difficult to activate, while its products are reactive and easily over-oxidised. In addition, it has low solubility in aqueous liquids and there are significant safety concerns due to the explosion risk [2,4].

Many researchers have addressed the challenge of the direct catalytic oxidation of methane. Most of this research has been focused on the direct formation of methanol by methane oxidation in the gas or liquid phase with O_2, N_2O, H_2O_2, or $H_2 + O_2$, as oxidant [5–11]. Acetic acid is another product of methane direct oxidation, but its selectivity is generally much lower than methanol [12]. Direct conversion to acetic acid is attractive since, although industrial production is an order of magnitude lower than methanol, it is an important chemical intermediate and as a C2 product it could potentially improve the carbon efficiency of the direct oxidation. In 2017 Flytzani-Stephanopoulos and coworkers demonstrated that introducing CO in the reaction system with Rh/ZSM-5 catalyst enhanced significantly the selectivity to acetic acid by direct oxidative carbonylation and improved the overall yield of

* Corresponding authors.
E-mail addresses: Hutch@cardiff.ac.uk (G.J. Hutchings), d.chadwick@imperial.ac.uk (D. Chadwick).

https://doi.org/10.1016/j.apcata.2025.120744
Received 26 September 2025; Received in revised form 9 December 2025; Accepted 10 December 2025
Available online 11 December 2025

liquid oxidation products. A maximum production of about 22,000 μmoles/g_{cat} acetic acid was achieved with 60–100 % selectivity in the liquid products [13]. The production of methanol was shown to follow a parallel pathway to the formation of acetic acid [13,14], while formic acid was produced either directly or from methanol by further oxidation [13,15]. Furthermore, it was shown that the CO ligand on Rh could act as a co-catalyst to promote oxygen insertion into activated methane to form methanol, or CO was inserted leading to the formation of acetic acid. In a later study of methane oxidation over Rh/ZSM-5, Moteki *et al.* [14] introduced the various reactant gases step-wise and again showed that CO plays important roles as ligands with Rh to form active catalyst sites and in the formation of surface oxo species. Besides Rh/ZSM-5, other metals in the platinum group and transition metals forming monometallic, bimetallic and trimetallic ZSM-5 catalyst systems have been tested in the direct oxidation of methane with the presence of CO, but overall Rh/ZSM-5 has shown superior activity in the production and selectivity of acetic acid [16–18].

Single atom Rh on ZSM-5 is the favoured catalyst for the formation of acetic acid by direct methane oxidative carbonylation with the C2/C1 ratio decreasing when Rh forms nanoparticles, typically above 0.5 wt% loading [13–15]. Reduced Rh/ZSM-5 shows higher selectivity towards acetic acid than calcined Rh/ZSM-5 catalysts, where the Rh_2O_3 species in calcined catalysts favours the formation of formic acid [15,19]. Wang *et al.* synthesised Al-free hydrophobic ZSM5-supported Rh catalysts which showed superior selectivity towards C1 products while the hydrophilic ZSM-5 supported Rh had higher selectivity towards acetic acid emphasising the importance of Brønsted acid sites [20]. Consequently, the addition of Na to Rh/ZSM-5 catalyst to lower the acid site concentration leads to a reduction of acetic acid formation [13]. Kolesnichenko *et al.* [21] using DFT calculations combined with the EXAFS modelling of Rh/ZSM-5 concluded that single-atom dispersed Rh associated with Al sites at channel intersections was probably the important catalytic species for acetic acid formation. Many researchers have demonstrated the importance of the support material to the selective production of oxygenates in methane oxidation, for example towards methanol [22–24].

In this work, the direct oxidation of low-concentration methane to acetic acid in aqueous phase has been investigated over zeolite-supported Rh catalysts in the presence of CO. C1 and C2 products were successfully produced at mild conditions at a higher production compared to previous work when correction is applied for the difference in methane pressures. ZSM-5 as support is compared to a range of commonly used zeolite frameworks [25,26], BEA, FAU, MOR, FER, and CHA, namely Z-beta, Z-Y, Mordenite, Ferrierite, and SSZ-13 respectively. This confirmed that ZSM5 yielded the highest C2/C1 ratio and production rate of acetic acid (969μmol/g_{cat}/h at the conditions used). Acetic acid production is shown to be maximum at a Si/Al ratio corresponding to ZSM5–50. The importance of the 3D channel structure of ZSM-5 in the high production of acetic acid is confirmed by a comparison with Rh supported on unidirectional ZSM23. The effect of Rh loading has been investigated, where the transition from isolated Rh to nanoparticles is demonstrated by TEM and CO-DRIFTS, and in methane oxidative carbonylation leads to lower production of acetic acid and a lower C2/C1 ratio as also reported by earlier studies. The competition with direct CO oxidation has been explored via the impact of gas composition on acetic acid and CO_2 production. A study of reaction conditions reveals that while C1 liquid products follow apparent first order kinetics, the production of acetic acid shows a strong dependence on pressure suggesting apparent second order or higher kinetics, the implications of which are discussed.

2. Experimental

2.1. Catalyst preparation

The Rh/zeolite catalysts were prepared using the incipient wetness impregnation method following the literature [13]. The various ammonia-form zeolites, ZSM-5, Zeolite Beta (Z-Beta), Zeolite Y (Z-Y), Mordenite (Mor.) and Ferrite (Fer.) were purchased from Zeolyst and used without further modification. The SiO_2/Al_2O_3 ratios are listed in Table 1. ZSM-23, and SSZ-13 were purchased from ACS materials and used without further modification. Rhodium(III) nitrate hydrate purchased from Sigma-Aldrich (36 % rhodium basis) was used as the rhodium (Rh) precursor.

In a typical preparation, the zeolite was pre-dried at 120 °C for 3 h to remove residual water from the internal pores. Rhodium nitrate solution was added slowly to the zeolite support. The resulting sample was then dried in an oven at 80 °C for 16 h. After drying, the sample was reduced in a 5 % H_2/N_2 flow at 550 °C for 3 h which reduced the Rh precursor to Rh and activated the zeolites from ammonia to H-form. The samples are denoted as x Rh/ZSM5-r, x is the Rh loading in weight percentage with a default value of 0.36 wt%, and r is the SiO_2/Al_2O_3 molar ratio with a default value of 30.

2.2. Catalyst characterisation

The Rh loading on the zeolites was determined by Inductively Coupled Plasma Optical Emission Spectroscopy (ICP-OES) by MEDAC Ltd using a Varian Vista MPX system. X-ray diffraction (XRD) spectra of the samples were collected using a PANalytical AERIS X-ray diffractometer with Cu Kα (λ=0.15418 nm) and the angle (2θ) ranged from 10 to 60°. N_2 adsorption and desorption isotherm of catalysts were obtained with a Tristar 3000; the surface area was calculated based on the Brunauer–Emmett–Teller (BET) method. Before the analysis, the reduced samples were pre-degassed in an N_2 environment at 300 °C overnight. XPS surface analysis of the catalysts was done using a Thermo K-Alpha X-ray Photoelectron Spectrometer (XPS) and an Al Kα source. The samples were mounted on carbon tape. C1s = 284.8 eV was used as the binding energy reference. TEM images were obtained with a JEM 2100 F and STEM-EDS was used for element mapping. H_2-TPR was obtained with a temperature programmed reaction system with a thermal conductivity detector (TCD) using 30 sccm of 5 % H_2/Ar heating up to 550 °C with ramping rate of 10 $Kmin^{-1}$. CO-DRIFT measurements were performed on a Thermo Nicolet 6700 instrument with a Hg–Cd–Te (MCT) detector and a Praying Mantis high-temperature reaction chamber with KBr windows. Samples were reduced in 100 sccm of 10 % H_2/He at 550°C for 30 min and cooled to room temperature in the IR cell and purged with He for 5 min. 100 sccm of 1 % CO/Ar gas was then flowed over the catalyst for 15 min where differential spectra were taken every 2 min using 64 scans and a resolution of 4 cm^{-1} to observe CO adsorption on Rh. 100 sccm of He was flowed again for 15 min to observe CO desorption from the Rh surface with spectra taken every 2 min.

2.3. Evaluation of catalyst performance

The reaction gas, consisting of 14.0 % CH_4, 3.5 % CO, 1.4 % O_2, and balance argon (Ar), was pre-mixed in a high-pressure burette. 10 mg of a Rh/zeolite catalyst and 10 g of deionized (DI) water were placed in a PTFE liner equipped with a Teflon coated cross bar stirrer and placed in a 25 ml high-pressure reactor (Buchi). The reactor was purged with

Table 1
Physicochemical properties of Rh/zeolite catalysts.

Code	MOR	FER	CHA	MFI	BEA	FAU
Zeolite	Mordenite	Ferrierite	SSZ-13	ZSM-5	Beta	Y
SiO_2/Al_2O_3	20	20	13–15	30	25	5.1
Rh loading (wt%)	0.31	0.42	0.40	0.36	0.42	0.34
Surface area (m^2/g)	427	286	580	389	551	418

argon before introducing the reaction gases and then pressurized to the desired pressure. Stirring speed was 600 rpm. The pressurized reactor was heated up to the reaction temperature using a temperature programmable, aluminium block heater. The time to reach the desired reaction temperature was typically 10 min. After reaction, the reactor was quickly immersed in an ice-water bath to halt the reaction process. The overhead gas components were collected using a gas sampling bag and analyzed using gas chromatography with a thermal conductivity detector (GC-TCD). NMR of the liquid products were examined with a Bruker AVANCE 500 NMR spectrometer after separating the catalyst. As for NMR analysis: typically, 0.9 g of experimental sample and 0.3 g of D_2O were mixed in an NMR tube. The identified oxygenated products were acetic acid (δ= 2.08 ppm), formic acid (δ= 8.44 ppm) and methanol (δ= 3.34 ppm) [15].

A deactivation study was carried out on 0.09 wt% Rh/ZSM-5 and 0.36 wt% Rh/ZSM-5 catalysts. After a 3-hour reaction, the catalyst was treated by the following methods. (1) The reactant liquid was removed and the spent catalyst was retained in the reactor, which was recharged with DI water and gas mixture for another 3-hour reaction. The recycled catalyst is denoted as "reused". (2) The catalyst was separated by centrifuge, dried and regenerated under 5 %H_2/N_2 at 550°C before the next run, which is denoted as "regenerated".

3. Results and discussion

3.1. Zeolite supports

It is well-known that the unique channel structure of zeolites can accommodate the catalytically active metal within the micropores and influence selectivity via the impact of the micropore dimensions and architecture [27,28]. Here, a range of Rh/zeolite-supported catalysts, including ZSM-5, Z-beta, Z-Y, mordenite, ferrierite and SSZ-13, have been compared in the direct oxidative carbonylation of low-concentration methane. The selected zeolite supports present a range of channel structures from one-dimensional (1D) to three-dimensional 3D with small (≤ 8 membered rings-MR), medium (10 MR) and large micropores (12MR). Their physiochemical properties are given in Table 1 and Table S1. While many have been studied previously in the context of direct methane oxidation [13–15], this is the first time to the authors knowledge that they have been systematically compared, and especially for direct oxidation of low-concentration methane.

According to the previous investigations of methane oxidation to acetic acid over Rh/ZSM-5, isolated Rh occurs at low loading, typically below 0.5 wt% Rh [13,14]. In the present study around 0.4 wt% Rh was used as the reference loading on the various zeolite supports (Table 1). This had no observable effect on the zeolite crystallinity based on the XRD patterns apart from the Rh/Z-Y catalyst, Fig. 1c. The hydrogen consumption in H_2-TPR for all the Rh/zeolite catalysts occurred mainly under 200 °C, Figure S1a, indicating that Rh is well-dispersed on the various zeolite supports [29].

The productivities of liquid and gas products for low concentration methane oxidative carbonylation in aqueous phase over the Rh/zeolites are shown in Fig. 2, and the carbon selectivity is listed in Table S2. All the measurements were made with the same CH_4: CO: O_2 initial ratio. Acetic acid, formic acid and methanol were the main liquid products with CO_2 as the sole gas product, as reported previously for the direct oxidation of high-concentration methane over Rh/ZSM-5 [13–15]. What is immediately striking is that ZSM5 is unique in presenting a high C2/C1 ratio – all the other zeolite supports present C2/C1 ratios below 1. Methanol and formic acid are the favoured products from Rh on the other zeolite supports. The total production of oxygenates is in the order of Rh/ZSM5 >>Rh/Z-Beta>Rh/Z-Y>Rh/Mor>Rh/Fer>Rh/SSZ13. This reflects the channel structure, pore size, and acidity of the zeolites. Once again ZSM5 is shown to be by far the best support for Rh-catalysed direct methane oxidation, especially to acetic acid.

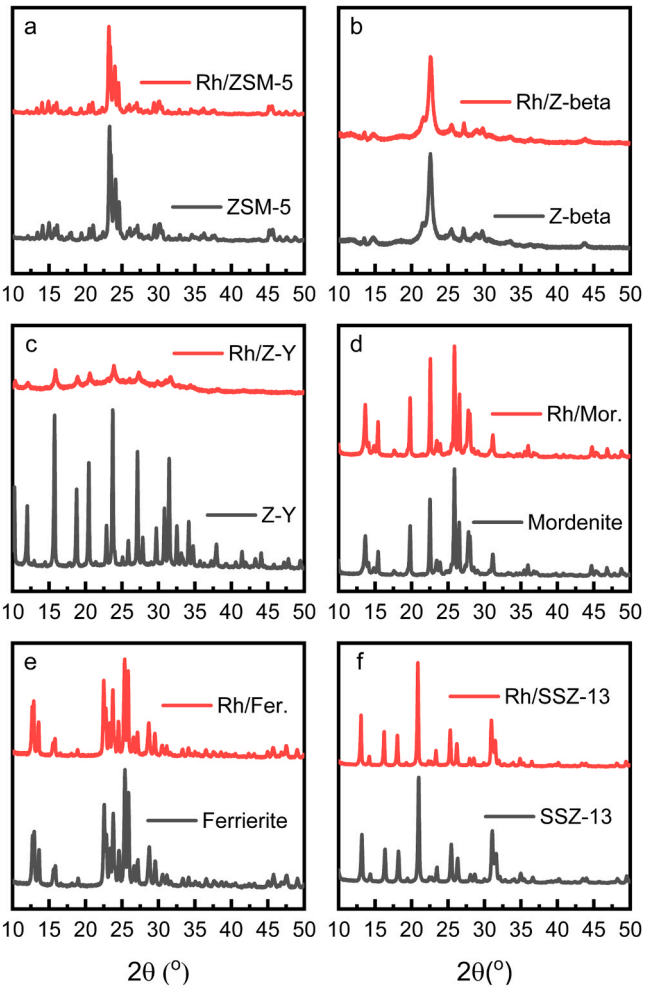

Fig. 1. XRD pattern of zeolite supports and Rh/zeolite catalysts (Rh loading given in Table 1).

For Rh/ZSM-5, the production of acetic acid, formic acid and methanol were 3245 μmol/$g_{cat.}$, 993 μmol/$g_{cat.}$, and 280 μmol/$g_{cat.}$, respectively, corresponding to a C2/C1 ratio ≈ 2.5. The superior selectivity to acetic acid over C1 products agrees well with the results of Flytzani-Stephanopoulos and coworkers [13] and others [17] obtained at high methane pressure. Allowing for the difference in methane pressures, the production rate of acetic acid (per bar CH_4 partial pressure and gram of Rh or per gram of catalyst) in the present work is higher than reported previously [13], Figure S2. Over Rh/ZSM-5 28281 μmol/$g_{cat.}$ of CO_2 was produced from the competing reaction pathway as expected [14], and is discussed further below in Section 3.5.

In general, the 3D zeolites (ZSM-5, Z-Beta, Z-Y) have greater production of oxygenates than the unidirectional or pseudo unidirectional channel zeolites (MOR and FER). Irrespective of the form of Rh in the zeolites, this probably reflects single-file diffusion effects in MOR and FER [30,31] since for oxidative carbonylation of methane three reactants must reach the same catalytic site and the product diffuse away.

Although Beta and Y zeolites possess 3D channels, their pore sizes are significantly larger than ZSM5. The lower production of oxygenates compared to Rh/ZSM5 is probably related to the formation of Rh nanoparticles and the nature of the adjacent acid sites of the supports. Generally, ZSM5 has stronger Brønsted acid sites compared to Beta and Y zeolites [32]. The active Rh species for oxidative carbonylation of methane in ZSM-5, at low Rh loading has been reported to be single atom dispersed Rh [13,15]. The larger pore size of Z-beta and Z-Y allows Rh nanoparticles to form at low loading, especially in the cages, leading

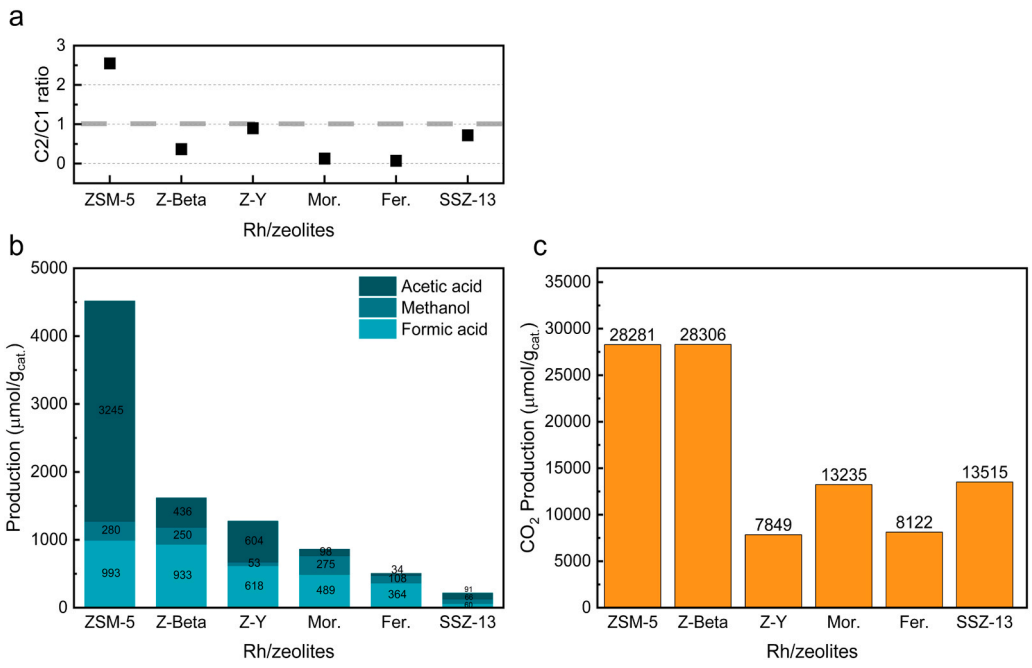

Fig. 2. Catalytic performance of Rh/zeolite catalysts, (a) C2/C1 liquid product ratio, (b) production of liquid products, and (c) production of CO_2. Corresponding carbon selectivity is listed in Table S2. (Reaction condition: 40 bar gas mixture containing about 5.6 bar CH_4, 0.56 bar O_2, 1.4 bar CO balanced in Ar, 10 g DI water, 10 mg Rh catalyst (Rh loading given in Table 1), 150°C, and 5 hr.).

to lower methane oxidation to acetic acid in particular. Additionally, the crystallinity and surface area of the reduced Rh/ZY catalyst were observed to be much lower than the original bulk Y zeolite, Fig. 1c, indicating some dealumination and framework collapse occurred during catalyst reduction [33].

Rh/SSZ-13 presented the lowest overall catalytic performance and a C2/C1 ratio less than 1. Moteki *et al.* [14] reported that Rh/SSZ-13 catalyst was selective for production of methanol from methane oxidation due to methane's smaller kinetic size (~0.36 nm [34]) compared to formic acid (~0.4 nm [35]) and acetic acid (~0.44 nm [35]) and the 0.38 nm pore mouth diameter of SSZ-13.

All the Rh/zeolite catalysts show a relatively high level of CO_2 production compared to liquid products, Fig. 2c. This arises mainly from the direct oxidation of CO as will be shown below in Section 3.5.

3.2. *Effect of the channel structure*

The influence of the 3-D vs 1-D channel structure was studied further by a direct comparison of Rh supported on ZSM5 and ZSM23 with almost the same SiO_2/Al_2O_3 ratio. This was done at the same Rh loading

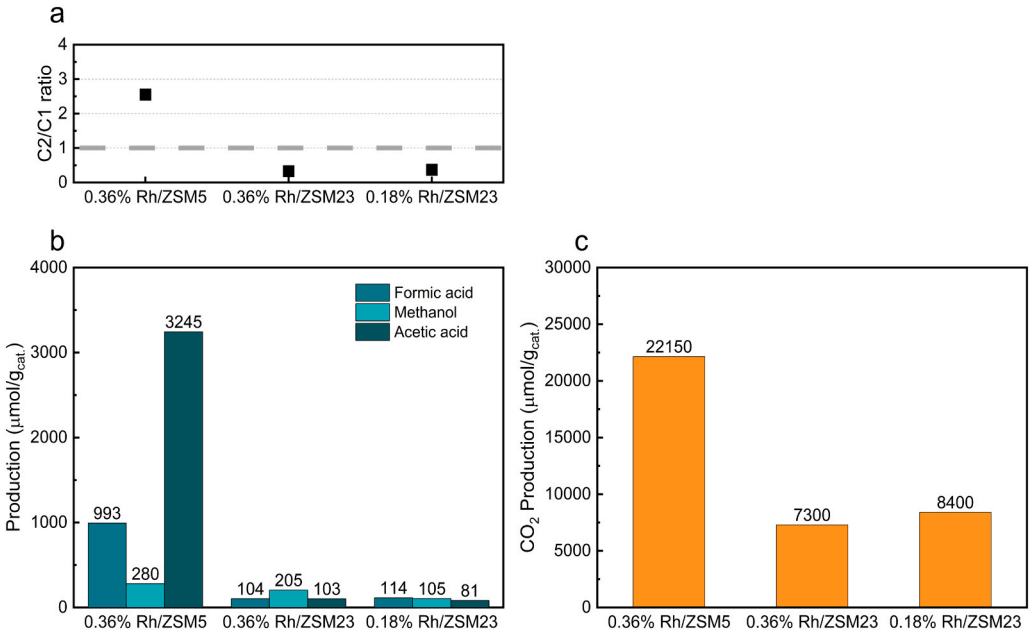

Fig. 3. Catalyst performance of Rh/ZSM5–30 and Rh/ZSM23–30, (a) C2/C1 ratio of liquid products, (b) production of liquid products, and (c) production of CO_2. Corresponding carbon selectivity is listed in Table S3. (Reaction condition: 40 bar gas mixture containing about 5.6 bar CH_4, 0.56 bar O_2, 1.4 bar CO balanced in Ar, 10 g DI water, 10 mg catalysts, 150°C, and 5 hr);.

initially, namely 0.36 wt% Rh. However, since the surface areas of ZSM5 and ZSM23 differ significantly, Table S1, a comparison is also made to Rh/ZSM23 with similar Rh loading per unit surface area, viz. 0.18 wt% Rh.

The addition of Rh was observed to have little effect on the crystallinity of ZSM23, see XRD in Figure S3. Evidence from XPS and H_2-TPR, Figure S4 and Figure S1b, suggests Rh on ZSM23 might aggregate to form nanoparticles [36,37]: the binding energy of Rh 3d 5/2 on ZSM23 (307.87 eV) is slightly higher than that on ZSM5 (307.54 eV), while the peak H_2 consumption temperature for Rh/ZSM23 is slightly higher than for Rh/ZSM5.

The catalytic performances of 0.36 wt% Rh/ZSM23 and 0.36 wt% Rh/ZSM5 are shown in Fig. 3 and Table S3, where the much lower production of acetic acid for 0.36 wt% Rh/ZSM23, 103 μmol/g_{cat}, compared to Rh/ZSM-5 is clearly seen. The C2/C1 ratio for the ZSM23 supported catalysts is also significantly less than 1, Fig. 3a, indicating Rh/ZSM23 catalysts are more selective towards C1 products. Results for 0.18 wt% Rh/ZSM-23, which as noted above, has similar Rh surface loading to 0.36 wt% Rh/ZSM5, present a similar picture with much lower production and greater selectivity to C1 products. These results confirm that the 3-D structure of ZSM-5 with its intersecting channels, plays an important role in achieving high selectivity to acetic acid by facilitating transport of the reactants to the active single atom Rh sites. As noted earlier DFT calculations and EXAFS modelling by Kolesnichenko et al. suggested that Rh anchored at Al sites at the channel intersections of ZSM-5 are the important catalytic sites for acetic acid formation [21], and the most energetically stable Al sites are located at the channel intersections [38,39]. In contrast, methane oxidation to acetic acid on Rh/ZSM23 without intersection channels is probably strongly influenced by single-file diffusion effects leading to reaction mainly on the outer surface or pore mouth [30] resulting in greater selectivity to C1 products and lower overall production. ZSM-23 was found previously to have greater catalytic activity in mono-reactant applications such as conversion of n-butanol to iso-butene [40].

3.3. ZSM5 SiO_2/Al_2O_3 ratio

The reference Rh loading, around 0.36 wt% (listed in Table S4), was introduced to ZSM-5 with different SiO_2/Al_2O_3 ratios (SAR), namely 23, 30, 50 and 80. Their catalytic performance is compared in Fig. 4 and Table S5. The acetic acid production showed volcano behaviour, rising with SAR to a peak at SAR = 50 followed by a fall at SAR = 80. CO_2 production largely due to direct CO oxidation (see below Section 3.5) also peaked at SAR = 50. The C1 liquid products, however, rose steadily with SAR showing no fall at SAR = 80. A consequence of this behaviour is that the C2/C1 ratio is > 2 while rising slightly to peak at SAR= 50 and then falls sharply to below 1 at SAR = 80. There are several potential factors at play here. Since the Rh loading is essentially constant, there may be an increase in the proportion of Rh nanoparticles formed as the number of available Al sites and Brønsted acid sites (BAS) decreases. Alternatively, or additionally, the number, location, spacing and distribution of Al sites and associated BAS may be the key factors.

To clarify the effect of SiO_2/Al_2O_3 ratio, a series of Rh/ZSM-5 catalysts with constant Rh/Al molar ratio were prepared and evaluated. A Rh/Al molar ratio around 0.02 was used with SAR = 23, 30, 50, 80. The acetic acid production per mol Rh is shown in Figure S5. The corresponding C2/C1 ratios, liquid oxygenate, and CO_2 productivities are reported in Figure S6a-c. The acetic acid production per mol Rh again shows volcano character with a peak at SAR = 50. In contrast, as above, the C1 liquid products increase steady with SAR. Consequently, the C2/C1 ratio again falls to about 1 at SAR = 80. And the CO_2 production per mol Rh now increases with SAR and does not show a maximum, Figure S6c. This would argue against increased Rh nanoparticle formation as SAR increases. Flytzani-Stephanopoulos *et al.* and others have demonstrated that the BAS are important in direct methane oxidation and especially in oxidative carbonylation to acetic acid [13,14]. As SAR increases, the number of Al sites and BAS decreases [40–43], and they become more widely spaced. However, the proton donor strength of the BAS increases [44,45]. In addition, the location of Al might also tend to favour the more stable T sites [39,46]. The observed volcano behaviour in the production of acetic acid with the maximum at SAR = 50 suggests that while for acetic acid production the increasing proton donor

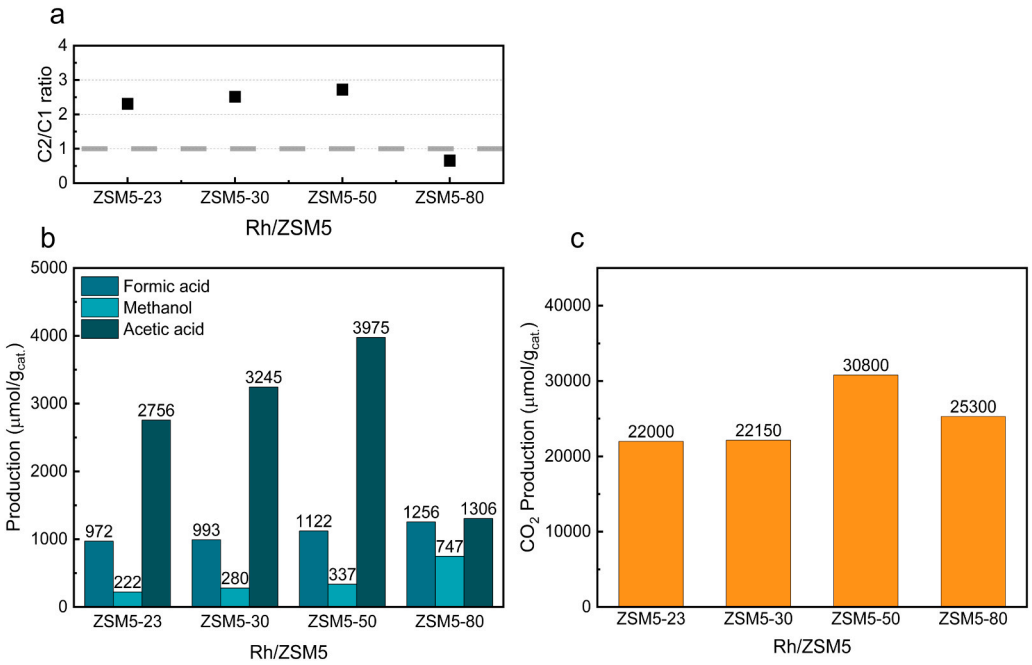

Fig. 4. Catalytic performance of Rh/ZSM5 with SiO_2/Al_2O_3 ratio of 23, 30, 50 and 80, (a) C2/C1 ratio of liquid products, (b) production of liquid products, (c) production of CO_2. Corresponding carbon selectivity is listed in Table S5. (Reaction condition: 40 bar gas mixture containing about 5.6 bar CH_4, 0.56 bar O_2, 1.4 bar CO balanced in Ar, 10 g DI water, 10 mg Rh catalysts, 150°C, and 5 hr).

strength of the BAS is important, the number, spacing and arrangement of neighbouring BAS is also important. Flytzani-Stephanopoulos and coworkers, while concluding that the BAS of ZSM-5 were essential for methane oxidation to acetic acid, implied that more than a single BAS per Rh(Al) was required [13]. Kolesnichenko *et al.* based on DFT calculations suggested that Rh at an Al site and a single associated BAS was the important catalytic site for acetic acid formation [21]. The present result would appear to favour the former interpretation. The formation of C1 liquid products, on the other hand, appears to respond to the increasing proton donor strength and requires only Rh at a single Al site and its associated BAS. It is tempting to speculate that this difference may be related to the fact that three reactants are required for methane oxidative carbonylation, while only two are required for C1 production. We show below in Section 3.6 below, that acetic acid production is strongly dependent on pressure consistent with a possible apparent 2nd order or higher kinetics, while the liquid C1 production is essentially apparent first order.

3.4. Rh loading

Since isolated Rh has been shown to be the active site for CH_4 oxidative carbonylation to acetic acid and behaves quite differently catalytically from Rh nanoparticles, which form with increasing loading and are reported to become dominant above 0.5 wt% Rh for impregnated catalysts [13,14], a series of catalysts with Rh loading from 0.09 wt% to 0.72 wt% were prepared and tested. ZSM5–30 was used as the support. 0.09 wt% Rh/ZSM5 showed the highest production of acetic acid of 5286 μmol/$g_{cat.}$ (or 5873 mmol/$g_{Rh.}$, Figure S7). The production of acetic acid gradually decreased with increasing Rh loading on ZSM5–0.72 wt%, Fig. 5b. The behaviour of the C2/C1 ratio was slightly different in that it went through a shallow maximum, Fig. 5a, and approached below 1 at the highest loading, 0.72 wt%. CO_2 production increased steadily to 0.36 wt% consistent with gradual formation of Rh nanoparticles, followed by a sharp increase when loading increased from 0.36 wt% to 0.72 wt%, consistent with extensive nanoparticle formation at the higher loading.

The effect of increased Rh loading on Rh dispersion was investigated by CO diffuse reflectance infrared Fourier transform spectroscopy (CO-DRIFTS), Fig. 6. The IR bands around 2068 cm^{-1} and 1899 cm^{-1} represent atop and bridged CO configurations on Rh nanoparticles [9, 13,47], while the peaks around 2115 cm^{-1} and 2050 cm^{-1} represent asymmetric and symmetric stretching of the dicarbonyl species $Rh^{+}(CO)_2$ where CO was adsorbed on isolated Rh species. The IR spectra could be deconvoluted satisfactorily into three peaks for 0.09 wt% Rh/ZSM5 catalysts and four peaks for 0.36 wt% Rh/ZSM5 and 0.72 wt% Rh/ZSM5 catalysts, Figure S8. With increasing Rh loading from 0.09 wt % to 0.72 wt%, the proportion of both asymmetric and symmetric stretching of dicarbonyl species dropped from 53 % and 38–23 % and 30 %, while the atop and bridged CO increased from 9 % and 0–30 % and 17 % confirming that the formation of Rh nanoparticles increases with Rh loading. TEM analysis, Fig. 7, showed that nanoparticles can be noticed at 0.18 wt% Rh/ZSM-5, but the number and size of Rh nanoparticles are observed to increase gradually with Rh loading, consistent

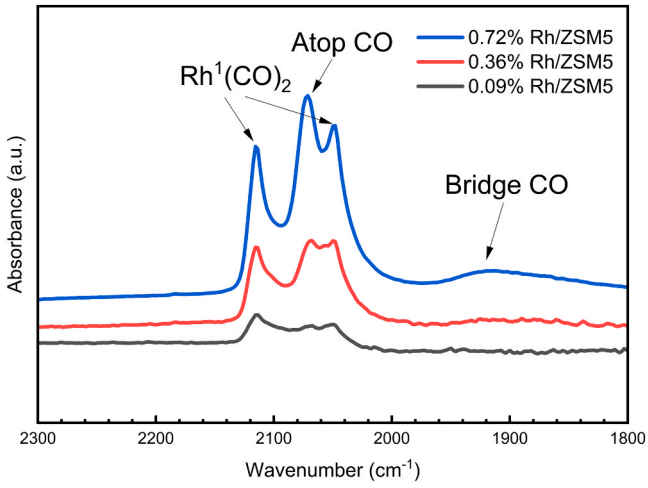

Fig. 6. CO-DRIFT spectra of Rh/ZSM5–30 with 0.09 wt%, 0.36 wt%, and 0.72 wt% Rh loading, respectively.

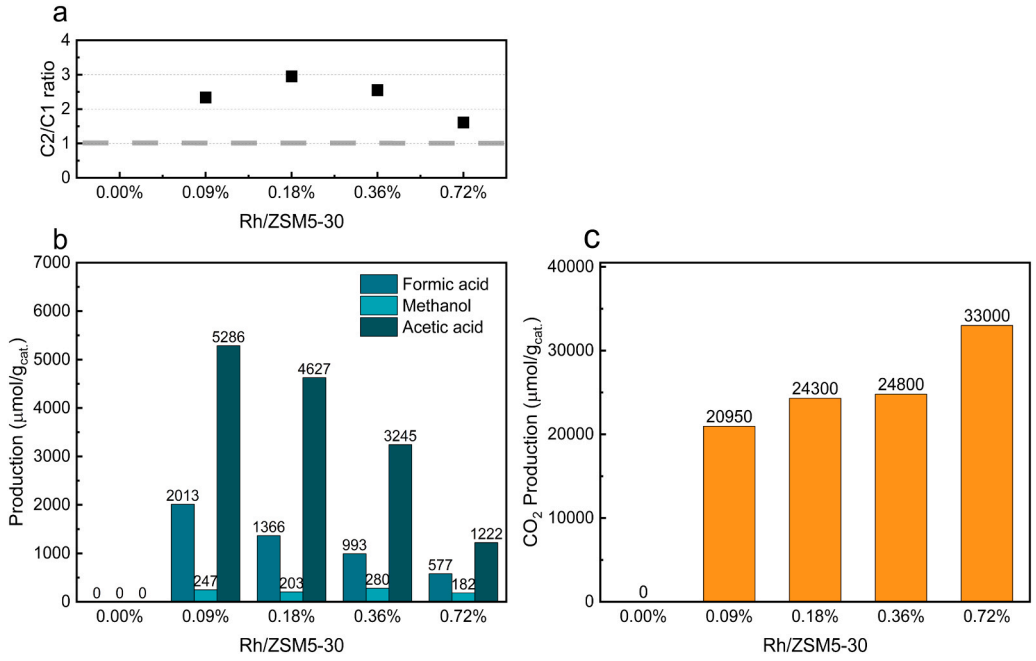

Fig. 5. Catalytic performance with various Rh loading on ZSM5–30 production rate per Rh loading, (a) C2/C1 ratio of liquid products, (b) production of liquid products, and (c) production of CO_2. Corresponding carbon selectivity is listed in Table S6. (Reaction condition: 40 bar gas mixture containing about 5.6 bar CH_4, 0.56 bar O_2, 1.4 bar CO balanced in Ar), 10 g DI water, 10 mg catalysts, 150°C, and 5 hr).

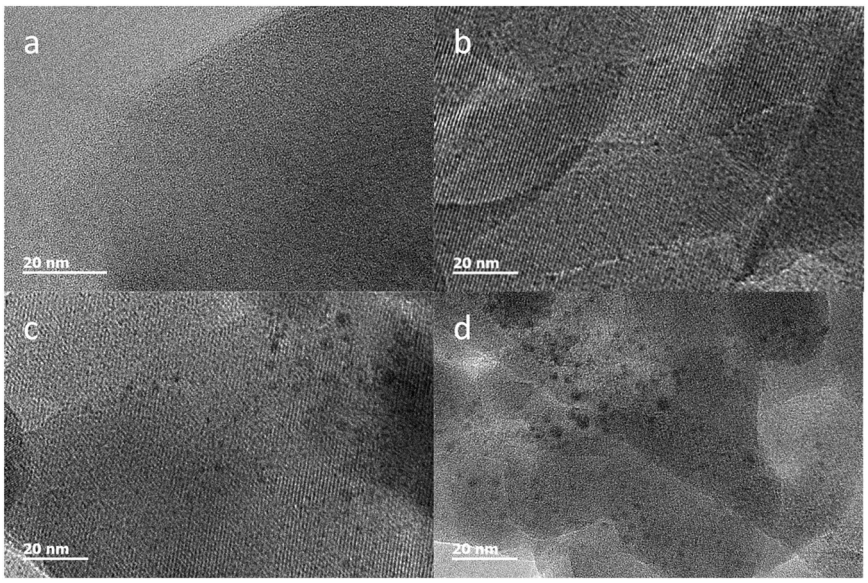

Fig. 7. TEM images: a. 0.09 wt% Rh/ZSM5–30; b. 0.18 wt% Rh/ZSM5; c. 0.36 wt% Rh/ZSM5; and d. 0.72 wt% Rh/ZSM5.

with the CO-DRIFTs results. In H_2-TPR (Figure S1c) the reduction temperature is observed to be shifted slightly to lower temperature with increasing Rh loading, due to the lower dispersion and correspondingly larger particle size [48, 49]. However not surprisingly, this is not reflected in XRD or XPS, Figure S9 and Figure S10, respectively. No obvious changes in crystallinity or binding energy for Rh/ZSM5 catalysts were found when the Rh loading increased from 0.09 wt% to 0.72 wt%, although the binding energy of Rh 3d5/2 for Rh/ZSM5 catalysts around 307.7 eV confirmed that Rh in the catalysts was fully reduced to its metal form as expected [50].

3.5. CO_2 production

The direct oxidative carbonylation of methane to acetic acid requires the addition of CO which is essential for the formation of C2 products and for promoting the reaction by coordination with Rh to form ^{1}Rh-$(CO)_2$ species [13–15]. However, CO_2 production also takes place which can occur both by overoxidation of liquid oxygenates and/or direct oxidation of methane and CO. As seen above, for example in Fig. 2, the undesired CO_2 production significantly exceeds liquid oxygenate production. To evaluate indirect CO_2 production Flytzani-Stephanopoulos and coworkers subtracted the CO_2 from direct oxidation to show that indirect CO_2 was around 5000 μmol/g_{cat} corresponding to a selectivity to liquid products of 60–100 % [13]. Moteki *et al.* reported more than 100 mol/mol_{Rh}/hr CO_2 was produced when CO is present in the reaction system [14]. A follow-up study found that most of the CO_2 was produced directly from CO oxidation [17]. In the present work, a series of reactant gas mixtures was applied to confirm the main reaction pathway for CO_2 production in low-pressure methane oxidation. The experiments were carried out multiple times, and the average values are listed in Table 2. The total pressure of a standard experiment in the present work was 40 bar containing about 5.6 bar CH_4, 0.56 bar O_2, 1.4 bar CO, and balanced in Argon (Case 1, Table 2). In Cases 2–4 listed below, the partial pressure of each component was maintained to be the same as that of the standard Case 1, and Ar was used to make up to the same total pressure of 40 bar. In Case 2, only CO and Ar were introduced to the reaction system and CO_2 production was less than 10 μmol corresponding to a production of less than 1000 μmol/g_{cat}. Adding O_2 into the reaction system, Case 3, significantly boosted the CO_2 production to 233 μmol corresponding to a production of 23300 μmol/g_{cat}. No H_2 production was found in either case indicating that production of CO_2 from the CO water gas shift reaction can be discounted. When no CO was present in the reaction gas, Case 4, the CO_2 production was less than 10 μmol or a production of less than 1000 μmol/g_{cat}. It is clear that more than 85 % CO_2 in direct oxidative carbonylation of methane is produced from direct CO oxidation at the conditions used. To reduce direct CO oxidation, alternative operating methodology such as sequential operation, or addition of catalyst promoters, might be effective ways to reduce CO_2 production and improve overall selectivity to liquid products.

Table 2
Catalytic performance using different reactant gases. (Reaction condition: 40 bar total pressure, 10 g DI water, 10 mg 0.36 wt% Rh/ZSM5-30, 150 °C, and 3 hr).

Case	Reactant gas in aqueous phase	Consumption [μmol]		Production [μmol]		Carbon balance (%)
		CH_4	CO	CO_2	C-liq	
1	$CH_4 + CO + O_2$	60	276	241	67	92 ± 3
2	CO	-	11	9	2	
3	$CO + O_2$	-	255	233	2	92 ± 2
4	$CH_4 + O_2$	-	-	7	2	

3.6. Reaction conditions

The reaction conditions have been varied to establish the impact on liquid oxygenate production, and in particular acetic acid. All the experiments have been carried out over 0.36 wt% Rh/ZSM5–30. Generally, the range of CH_4 pressures studied in the literature has been between 20 and 50 bar to obtain around 150–270 μmol acetic acid in a typical reaction time [13,15]. As the focus of interest in the present study is low-concentration methane, methane partial pressure has been extended over a range of 2 – 5 bar with a fixed CH_4:CO:O_2 ratio (10:2.5:1). The total pressure and corresponding partial pressures of CH_4, CO and O_2 can be found in Table S7. The production of liquid products is shown in Fig. 8a (acetic acid in x-y form in Figure S11); the corresponding CO_2 production can be found in Figure S12a. Methanol production was always the lowest within the pressure range. This result is consistent with the literature where the production of methanol is found to be the lowest among formic acid and acetic acid in CH_4, CO and O_2 reaction systems, and where CH_3OH could be oxidised to HCOOH [15]. The production of acetic acid increased significantly with an increase in methane partial pressure and total pressure as expected; the

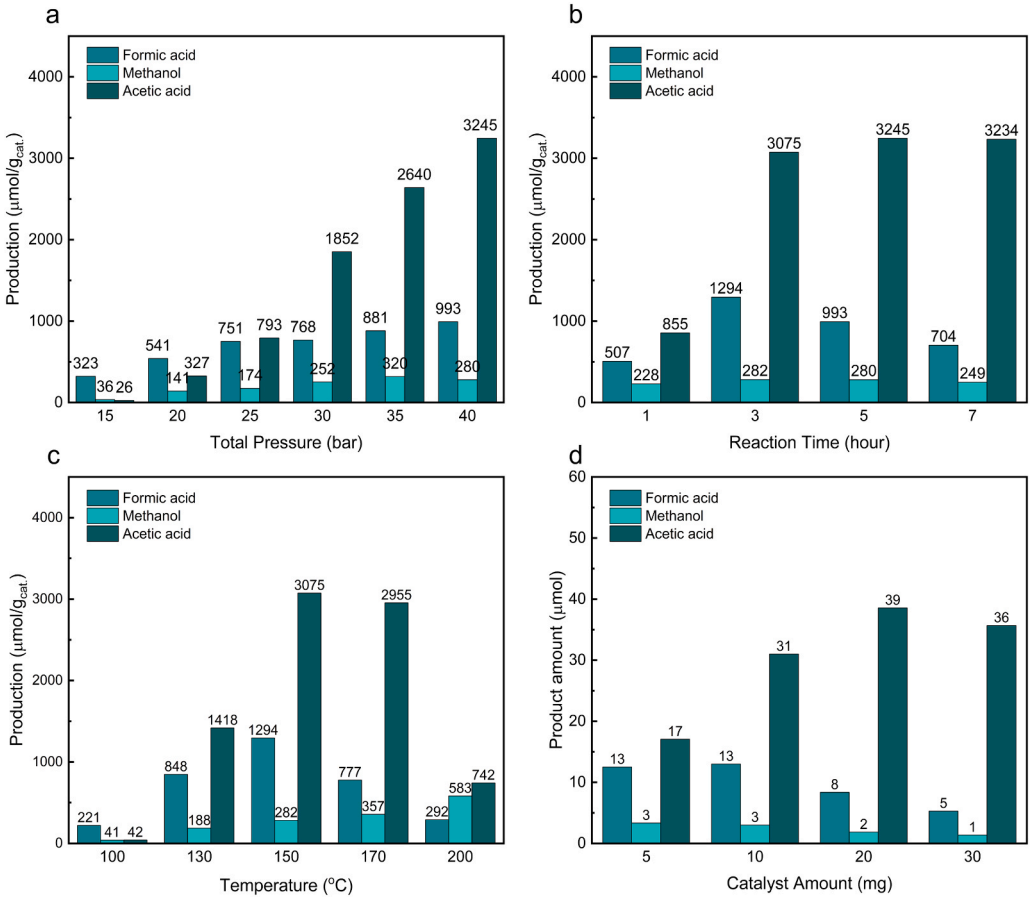

Fig. 8. Catalytic performance at different conditions: (a) total pressure in a range of 15–40 bar; (b) reaction time between 1 and 7 h; (c) temperature in a range of 100–200 °C; (d) catalyst amount in a range of 5–30 mg. (Reaction condition: 0.36 wt% Rh/ZSM5–30 catalyst, (a) 10 mg catalyst, 150 °C, 5 hr, reactant gas pressure listed in Table S7; (b) 40 bar reactant gas (5.6 bar CH_4, 0.56 bar O_2, 1.4 bar CO balanced in Ar), 10 mg catalyst, 150 °C; (c) 40 bar reactant gas, 10 mg catalysts, 3 hr; (d) 40 bar reactant gas, 150°C, 3 hr.). Corresponding carbon selectivity is listed in Table S9-S12.

production of the C1 liquid products methanol and formic acid increased more gradually. CO_2 production increased with total pressure to 30 bar and then appeared to plateau. Formic acid was the dominant liquid product at total pressures below 25 bar, while acetic acid became increasingly the dominant product when the total pressure exceeded 25 bar. Consequently, the liquid product C2/C1 ratio rises continuously as pressure increases, Figure S13a. Overall, the acetic acid production shows a strong dependence on pressure consistent with an approximately second order or higher dependence on pressure, Figure S14, while the C1 liquid production appears to be apparent first order. Note that the CH_4:CO:O_2 partial pressure ratio is fixed to 10:2.5:1. This difference in the apparent kinetics of acetic acid and liquid C1 products could be interpreted as the involvement of two or more kinetically significant species in direct oxidative carbonylation and one kinetically significant species in the case of liquid C1 production. Clearly, the difference in the pressure dependence of C1 and C2 liquid products presents a challenge for direct oxidation to acetic acid of low concentration methane.

Reaction time was also varied from 1 h to 7 h at fixed total pressure (40 bar) and gas composition. The production of liquid products is shown in Fig. 8b (acetic acid x-y form in Figure S11b); the production of CO_2 is shown in Figure S12b. The formation of acetic acid significantly increased from 1 to 3 h reaction time tending to a plateau at longer reaction time. This can result from several factors including catalyst deactivation and/or the consumption of reactants – for example of CO since this also undergoes parallel direct oxidation. The observed change in total reaction pressure during reaction and composition was negligible. Hence, limitation of reactants can be eliminated as the cause of the plateau under the present reaction conditions.The production of formic acid reached a maximum at 3 h reaction time, decreasing thereafter, consistent with further oxidation to CO_2 which is observed to rise continuously. This causes the C2/C1 liquid product ratio to rise continuously with reaction time, Figure S13b. Methanol production was always low so no definitive trend could be observed. Analysis of the present reaction fluid after a typical 3 hr run confirmed that no Rh was leached into the water, which agrees with Flytzani-Stephanopoulos and coworkers [13]. It seems likely that the cause of the observed plateau in acetic acid production at extended reaction times in the present study is catalyst deactivation (see below).

The catalytic performance at various temperatures from 100 °C to 200 °C is shown in Fig. 8c, Figure S11c and Figure S12c. The production of acetic acid and formic acid, and the production of CO_2, peaked at a reaction temperature of 150 °C; the production of methanol appeared to grow continuously with increasing reaction temperature although it is always low. The C2/C1 ratio decreased above 170 °C, Figure S13c. These observations are consistent with the literature [19]. Increase in reaction temperature above 150 °C without an increase in pressure would significantly reduce the reactant gas solubility which could led to a decrease in the rate of product formation.

The effect of the catalyst amount on catalytic performance is shown in Fig. 8d, Figure S11d - S13d. The production of acetic acid increased with increasing catalyst amount from 5 mg to 20 mg, then reached a plateau. At high catalyst concentrations, the reaction would likely become increasingly limited by mass transfer at the reactant pressures used in the present work. In principle, this could be alleviated by a suitable method of process intensification. Recently, Aurnob et al. [51]

reported on the gas phase methane oxidative carbonylation over Rh/ZSM-5. A gas-solid catalytic process could in principle alleviate mass transfer concerns. However, the present gas-liquid phase reaction results show much higher productivity (μmol/g_{cat}/h) of acetic acid with higher C-selectivity, and lower CO_2 production.

The catalytic performance of reused and regenerated catalysts suffered over 90 % and 70 % drop in acetic acid production, respectively, Table S8. TEM analysis, Figure S15, indicated that Rh particles were strongly aggregated following the first 3-hour reaction, suggesting a loss of isolated Rh active sites. The regenerated Rh/ZSM-5 catalyst showed improvement in catalytic performance compared to the reused catalyst, but favoured C1 production. Development of a more stable catalyst and/or an improved recycling procedure is needed for future applications.

4. Conclusion

The direct catalytic oxidation of methane in the presence of CO was successfully converted to C1 and C2 products over Rh/ZSM-5 with high selectivity to acetic acid. Emphasis has been placed on relatively low concentration methane compared to earlier work as this offers a potential route to conversion of waste methane. The acetic acid production was higher than reported by Flytzani-Stephanopoulos and coworkers [13] when allowance is made for the difference in pressures. However, above 85 % CO_2 production was found to be formed from direct CO oxidation in low-pressure methane oxidation with CO present, the balance being from deeper oxidation of the liquid C1 products. ZSM-5 supported Rh showed the highest production and selectivity of acetic acid with a C2/C1 ratio$>$ 1 compared to a range of Rh/zeolite catalysts, including Z-Beta, Z-Y, MOR, FER, and SSZ-13. The importance of the 3-D channel structure of the zeolite support was confirmed by a direct comparison with Rh/ZSM-23 catalysts with similar Si/Al ratio and surface Rh loading. It seems likely that unidirectional zeolites experience single-file diffusion effects which result in the outer surface and the pore mouth making the greater contribution to methane conversion.

A study of the effect of SiO_2/Al_2O_3 ratio of ZSM-5 from 23 to 80 showed that Rh/ZSM5–50 gave the highest production and selectivity to acetic acid, even when the Rh/Al ratio was maintained constant for the various SiO_2/Al_2O_3 ratios. By contrast the C1 liquid products increased with SiO_2/Al_2O_3 ratio showing no maximum. The fall in acetic acid production when the SiO_2/Al_2O_3 ratio exceeded 50 suggests that interaction between the single atom dispersed Rh at the Al site and the surrounding BAS of the support (rather than just the single BAS associated with the Al site) is important in the formation of acetic acid. This observation is consistent with acetic acid production showing a strong dependence on pressure consistent with apparent second order or higher kinetics.

From an investigation of Rh loading 0.09 wt% Rh/ZSM5 presented the highest production of acetic acid. Increasing Rh loading resulted in a steady drop of production of liquid oxygenates consistent with gradual formation of Rh nanoparticles, and a sharp fall at high Rh loading. The formation of Rh nanoparticles was confirmed by CO-DRIFTS and TEM.

The strong dependence on pressure of acetic acid production was such that to obtain a C2/C1 liquid product ratio above 1, a minimum methane pressure of 3.5 bar is needed at the conditions used. Aggregation of Rh species during reaction leads to the catalyst deactivation, which can not be reversed by H_2 reduction. The findings in the present work can encourage the design of more stable catalysts, process intensification approaches to improve acetic acid production and reduce CO_2 production, and guide the development of practical catalytic processes for low-carbon chemical manufacturing.

CRediT authorship contribution statement

Olukayode Gideon Oloyede: Methodology, Investigation. **Jialin Yu:** Writing – review & editing, Writing – original draft, Methodology, Investigation. **Kunlun Ding:** Writing – review & editing, Supervision, Resources, Project administration, Methodology, Funding acquisition, Conceptualization. **Berko Mark B. F.:** Writing – review & editing, Methodology, Investigation. **Richard J. Lewis:** Writing – review & editing, Project administration, Methodology. **David Chadwick:** Writing – review & editing, Supervision, Resources, Project administration, Methodology, Funding acquisition, Conceptualization. **Graham J. Hutchings:** Writing – review & editing, Project administration, Methodology, Funding acquisition, Conceptualization. **Stuart H. Taylor:** Writing – review & editing, Resources, Project administration, Methodology, Funding acquisition, Conceptualization. **Kang Li:** Writing – review & editing, Supervision, Resources, Project administration, Methodology, Funding acquisition, Conceptualization.

Declaration of Competing Interest

The authors declare that they have no known competing financial interests or personal relationships that could have appeared to influence the work reported in this paper.

Acknowledgement

The authors thank Peter Haycock and Stuart J. Elliott for their contributions in conducting NMR experiments and providing professional advice, and Mahmoud G. Ardakani and Ecaterina Ware for their assistance with TEM analysis. The authors acknowledge the financial support from UK EPSRC EP/W014408/1 and from U.S. NSF 2302161.

Appendix A. Supporting information

Supplementary data associated with this article can be found in the online version at doi:10.1016/j.apcata.2025.120744.

Data Availability

No data was used for the research described in the article.

References

[1] IEA, Methane Tracker 2021, Paris, 2021. ⟨https://www.iea.org/reports/methane-tracker-2021⟩.
[2] X. Wang, F. Zhou, Y. Ling, Y. Xiao, B. Ma, X. Ma, S. Yu, H. Liu, K. Wei, J. Kang, Overview and outlook on utilization technologies of low-concentration coal mine methane, Energy Fuels 35 (2021) 15398–15423, https://doi.org/10.1021/acs.energyfuels.1c02312.
[3] F. Yin, B. Nie, Y. Wei, S. Lin, Co-production system based on lean methane and biogas for power generation in coal mines, Atmosphere 13 (2022) 1–16, https://doi.org/10.3390/atmos13050803.
[4] Y. Yang, T. Li, P. Feng, X. Wang, S. Wang, Y. Ling, Z. Shao, Highly efficient conversion of oxygen-bearing low concentration coal-bed methane into power via solid oxide fuel cell integrated with an activated catalyst-modified anode microchannel, Appl. Energy 328 (2022) 120134, https://doi.org/10.1016/j.apenergy.2022.120134.
[5] E. Tabor, M. Lemishka, Z. Sobalik, K. Mlekodaj, P.C. Andrikopoulos, J. Dedecek, S. Sklenak, Low-temperature selective oxidation of methane over distant binuclear cationic centers in zeolites, Commun. Chem. 2 (2019) 1–9, https://doi.org/10.1038/s42004-019-0173-9.
[6] L. Tao, I. Lee, R. Khare, A. Jentys, J.L. Fulton, M. Sanchez-Sanchez, J.A. Lercher, Speciation of Cu-Oxo clusters in ferrierite for selective oxidation of methane to methanol, Chem. Mater. 34 (2022) 4355–4363, https://doi.org/10.1021/acs.chemmater.1c04249.
[7] C.W. Wang, Y. Sun, L.J. Wang, W.H. Feng, Y.T. Miao, M.M. Yu, Y.X. Wang, X. D. Gao, Q. Zhao, Z. Ding, Z. Feng, S.M. Yu, J. Yang, Y. Hu, J.F. Wu, Oxidative carbonylation of methane to acetic acid on an Fe-modified ZSM-5 zeolite, Appl. Catal. B Environ. 329 (2023) 122549, https://doi.org/10.1016/j.apcatb.2023.122549.
[8] N. Agarwal, S.J. Freakley, R.U. Mcvicker, S.M. Althahban, N. Dimitratos, Q. He, D. J. Morgan, R.L. Jenkins, D.J. Willock, S.H. Taylor, C.J. Kiely, G.J. Hutchings, Aqueous Au-Pd colloids catalyze selective CH4 oxidation to CH3OH with O 2 under mild conditions, Science 358 (80) (2017) 223–227.
[9] S. Al-Shihri, C.J. Richard, D. Chadwick, Selective oxidation of methane to methanol over ZSM-5 catalysts in aqueous hydrogen peroxide: role of formaldehyde, ChemCatChem 9 (2017) 1276–1283, https://doi.org/10.1002/cctc.201601563.
[10] J. Kim, J.H. Kim, C. Oh, H. Yun, E. Lee, H.S. Oh, J.H. Park, Y.J. Hwang, Electro-assisted methane oxidation to formic acid via in-situ cathodically generated H2O2

under ambient conditions, Nat. Commun. 14 (2023), https://doi.org/10.1038/s41467-023-40415-6.
[11] C. Hammond, M.M. Forde, M.H. AbRahim, A. Thetford, Q. He, R.L. Jenkins, N. Dimitratos, J.A. Lopez-Sanchez, N.F. Dummer, D.M. Murphy, A.F. Carley, S. H. Taylor, D.J. Willock, E.E. Stangland, J. Kang, H. Hagen, C.J. Kiely, G. J. Hutchings, Direct catalytic conversion of methane to methanol in an aqueous medium by using copper-promoted Fe-ZSM-5, Angew. Chem. Int. Ed. 51 (2012) 5129–5133, https://doi.org/10.1002/anie.201108706.
[12] N.F. Dummer, D.J. Willock, Q. He, M.J. Howard, R.J. Lewis, G. Qi, S.H. Taylor, J. Xu, D. Bethell, C.J. Kiely, G.J. Hutchings, Methane oxidation to methanol, Chem. Rev. 123 (2023) 6359–6411, https://doi.org/10.1021/acs.chemrev.2c00439.
[13] J. Shan, M. Li, L.F. Allard, S. Lee, M. Flytzani-Stephanopoulos, Mild oxidation of methane to methanol or acetic acid on supported isolated rhodium catalysts, Nature 551 (2017) 605–608, https://doi.org/10.1038/nature24640.
[14] T. Moteki, N. Tominaga, M. Ogura, Mechanism investigation and product selectivity control on CO-assisted direct conversion of methane into C1 and C2 oxygenates catalyzed by zeolite-supported Rh, Appl. Catal. B Environ. 300 (2022) 120742, https://doi.org/10.1016/j.apcatb.2021.120742.
[15] Y. Tang, Y. Li, V. Fung, D.E. Jiang, W. Huang, S. Zhang, Y. Iwasawa, T. Sakata, L. Nguyen, X. Zhang, A.I. Frenkel, F. Tao, Single rhodium atoms anchored in micropores for efficient transformation of methane under mild conditions, Nat. Commun. 9 (2018) 1–11, https://doi.org/10.1038/s41467-018-03235-7.
[16] T.I. Batova, A.N. Stashenko, T.K. Obukhova, Y.M. Snatenkova, E.V. Khramov, A. A. Sadovnikov, K.B. Golubev, N.V. Kolesnichenko, Oxidative carbonylation of methane into acetic acid: Effect of metal (Zn, Cu, La, and Mg) doping on Rh/ZSM-5 activity, Microporous Mesoporous Mater. 366 (2024) 112953, https://doi.org/10.1016/j.micromeso.2023.112953.
[17] T. Moteki, N. Tominaga, M. Ogura, CO-assisted direct methane conversion into C1 and C2 oxygenates over ZSM-5 supported transition and platinum group metal catalysts using oxygen as an oxidant, ChemCatChem 12 (2020) 2957–2961, https://doi.org/10.1002/cctc.202000168.
[18] M. Li, J. Shan, G. Giannakakis, M. Ouyang, S. Cao, S. Lee, L.F. Allard, M. Flytzani-Stephanopoulos, Single-step selective oxidation of methane to methanol in the aqueous phase on iridium-based catalysts, Appl. Catal. B Environ. 292 (2021) 120124, https://doi.org/10.1016/j.apcatb.2021.120124.
[19] X. Yu, J. Mao, B. Wu, Y. Wei, Y. Sun, L. Zhong, Boosting direct oxidation of methane with molecular oxygen at low temperature over Rh/ZSM-5 catalyst, ChemCatChem 15 (2023) 1–7, https://doi.org/10.1002/cctc.202300077.
[20] H. Wang, W. Xin, Q. Wang, X. Zheng, Z. Lu, R. Pei, P. He, X. Dong, Direct methane conversion with oxygen and CO over hydrophobic dB-ZSM-5 supported Rh single-atom catalyst, Catal. Commun. 162 (2022) 106374, https://doi.org/10.1016/j.catcom.2021.106374.
[21] N.V. Kolesnichenko, T.I. Batova, A.N. Stashenko, T.K. Obukhova, E.V. Khramov, A. A. Sadovnikov, D.E. Zavelev, The role of the spatial arrangement of single rhodium sites on ZSM-5 in the oxidative methane carbonylation to acetic acid, Microporous Mesoporous Mater. 344 (2022) 112239, https://doi.org/10.1016/j.micromeso.2022.112239.
[22] B.E.R. Snyder, M.L. Bols, H.M. Rhoda, D. Plessers, R.A. Schoonheydt, B.F. Sels, E. I. Solomon, Cage effects control the mechanism of methane hydroxylation in zeolites, Science 373 (80) (2021) 327–331, https://doi.org/10.1126/science.abd5803.
[23] M.L. Bols, J. Devos, H.M. Rhoda, D. Plessers, E.I. Solomon, R.A. Schoonheydt, B. F. Sels, M. Dusselier, Selective formation of α-Fe(II) sites on Fe-Zeolites through one-pot synthesis, J. Am. Chem. Soc. 143 (2021) 16243–16255, https://doi.org/10.1021/jacs.1c07590.
[24] D. Plessers, A.J. Heyer, H.M. Rhoda, M.L. Bols, E.I. Solomon, R.A. Schoonheydt, B. F. Sels, Tuning copper active site composition in Cu-MOR through Co-cation modification for methane activation, ACS Catal. 13 (2023) 1906–1915, https://doi.org/10.1021/acscatal.2c05271.
[25] R. Bingre, B. Louis, P. Nguyen, An overview on zeolite shaping technology and solutions to overcome diffusion limitations, Catalysts 8 (2018), https://doi.org/10.3390/catal8040163.
[26] Y. Li, L. Li, J. Yu, Applications of zeolites in sustainable chemistry, Chem 3 (2017) 928–949, https://doi.org/10.1016/j.chempr.2017.10.009.
[27] Y. Wang, C. Wang, L. Wang, L. Wang, F.S. Xiao, Zeolite fixed metal nanoparticles: new perspective in catalysis, Acc. Chem. Res. 54 (2021) 2579–2590, https://doi.org/10.1021/acs.accounts.1c00074.
[28] H. Wang, L. Wang, F.S. Xiao, Metal@zeolite hybrid materials for catalysis, ACS Cent. Sci. 6 (2020) 1685–1697, https://doi.org/10.1021/acscentsci.0c01130.
[29] H. Jeong, G. Lee, B.S. Kim, J. Bae, J.W. Han, H. Lee, Fully dispersed Rh ensemble catalyst to enhance low-temperature activity, J. Am. Chem. Soc. 140 (2018) 9558–9565, https://doi.org/10.1021/jacs.8b04613.
[30] J. Kärger, Structure-Related Diffusion in Nanoporous Materials (Access), in: T. J. Pinnavaia, M.F. Thorpe (Eds.), Nanoporous Mater, Springer US, Boston, MA, 2002, pp. 175–193, ⟨https://doi.org/10.1007/0-306-47066-7_12⟩ (Access).
[31] J.A.Z. Pieterse, K. Seshan, J.A. Lercher, Structure-activity correlations for TON, FER, and MOR in the hydroisomerization of n-butane, J. Catal. 195 (2000) 326–335, https://doi.org/10.1006/jcat.2000.3003.
[32] F. Mirshafiee, R. Karimzadeh, R. Khoshbin, Effect of textural properties of Y, ZSM-5 and beta zeolites on their catalytic activity in catalytic cracking of a middle distillate cut named RCD, beta zeolites, J. Oil Gas. Petrochem. Technol. 8 (2021) 60–74, https://doi.org/10.22034/JOGPT.2022.273313.1092.1.
[33] N. Salman, C.H. Rüscher, J.C. Buhl, W. Lutz, H. Toufar, M. Stöcker, Effect of temperature and time in the hydrothermal treatment of HY zeolite, Microporous Mesoporous Mater. 90 (2006) 339–346, https://doi.org/10.1016/j.micromeso.2005.09.032.
[34] Y. Tang, D. Dubbeldam, S. Tanase, Water-ethanol and methanol-ethanol separations using in situ confined polymer chains in a metal-organic framework, ACS Appl. Mater. Interfaces 11 (2019) 41383–41393, https://doi.org/10.1021/acsami.9b14367.
[35] J.M. Crawford, J.B. Jasinski, M.A. Carreon, Towards continuous deoxygenation of acetic acid catalyzed by recyclable mono/bi/trimetallic zeolite catalysts, J. Catal. 401 (2021) 137–148, https://doi.org/10.1016/j.jcat.2021.07.018.
[36] B. Kang, R. Zhang, M. Guo, X. Guo, Z. Di, Y. Wei, J. Jia, Topological aspect of the distribution of Co species and N2O decomposition performance for Co/zeolite catalysts, Energy Fuels 37 (2023) 18019–18029, https://doi.org/10.1021/acs.energyfuels.3c01958.
[37] K.S. Shinkevich, R.G. Kukushkin, O.A. Bulavchenko, O.O. Zaikina, M.V. Alekseeva, P.S. Ruvinskiy, V.A. Yakovlev, Influence of the support on activity and stability of Ni and Ni-Mo catalysts in the hydroprocessing of fatty acids into motor fuels components, Appl. Catal. A Gen. 644 (2022) 118801, https://doi.org/10.1016/j.apcata.2022.118801.
[38] R.J. Bunting, J. Thompson, P. Hu, The mechanism and ligand effects of single atom rhodium supported on ZSM-5 for the selective oxidation of methane to methanol, Phys. Chem. Chem. Phys. 22 (2020) 11686–11694, https://doi.org/10.1039/d0cp01284j.
[39] A. Ghorbanpour, J.D. Rimer, L.C. Grabow, Periodic, vdW-corrected density functional theory investigation of the effect of Al siting in H-ZSM-5 on chemisorption properties and site-specific acidity, Catal. Commun. 52 (2014) 98–102, https://doi.org/10.1016/j.catcom.2014.04.005.
[40] D. Zhang, S.A.I. Barri, D. Chadwick, N-Butanol to iso-butene in one-step over zeolite catalysts, Appl. Catal. A Gen. 403 (2011) 1–11, https://doi.org/10.1016/j.apcata.2011.05.037.
[41] S.M. Opalka, T. Zhu, Influence of the Si/Al ratio and Al distribution on the H-ZSM-5 lattice and Brønsted acid site characteristics, Microporous Mesoporous Mater. 222 (2016) 256–270, https://doi.org/10.1016/j.micromeso.2015.10.030.
[42] C.N.F. Ramôa Ribeiro, Alírio E. Rodrigues, L. Deane Rollmann. Zeolites: Science and Technology, 1st ed., Springer, Dordrecht, 1984 https://doi.org/10.1007/978-94-009-6128-9.
[43] S. Siahrostami, H. Falsig, P. Beato, P.G. Moses, J.K. Nørskov, F. Studt, Exploring scaling relations for chemisorption energies on transition-metal-exchanged zeolites ZSM-22 and ZSM-5, ChemCatChem 8 (2016) 767–772, https://doi.org/10.1002/cctc.201501049.
[44] F. Gu, X. Qin, L. Pang, R. Zhang, M. Peng, Y. Xu, S. Hong, J. Xie, M. Wang, D. Han, D. Xiao, G. Guo, X. Wang, Z. Wang, D. Ma, Acid-promoted selective oxidation of methane to formic acid over dispersed rhodium catalysts under mild conditions, ACS Catal. 13 (2023) 9509–9514, https://doi.org/10.1021/acscatal.3c01743.
[45] A.H. Clark, H.R. Marchbank, D. Thompsett, J.M. Fisher, A. Longo, K.A. Beyer, T. I. Hyde, G. Sankar, On the effect of metal loading on the reducibility and redox chemistry of ceria supported Pd catalysts, Phys. Chem. Chem. Phys. 24 (2022) 2387–2395, https://doi.org/10.1039/d1cp04654c.
[46] F. Barzegari, F. Farhadi, M. Rezaei, M. Kazemeini, A. Keshavarz, Influence of metal loading and reduction temperature on the performance of mesoporous NiO–MgO–SiO2 catalyst in propane steam reforming, J. Energy Inst. 96 (2021) 38–51, https://doi.org/10.1016/j.joei.2021.01.013.
[47] B. Fan, M. Jiang, G. Wang, Y. Zhao, B. Mei, J. Han, L. Ma, C. Li, G. Hou, T. Wu, L. Yan, Y. Ding, Elucidation of hemilabile-coordination-induced tunable regioselectivity in single-site Rh-catalyzed heterogeneous hydroformylation, Nat. Commun. 15 (2024), https://doi.org/10.1038/s41467-024-51281-1.